Clays and Clay Minerals, Vol. 59, No. 6, 608–616, 2011.

ILLITE FROM MULOORINA, SOUTH AUSTRALIA

RICHARD A. EGGLETON AND JOHN FITZ GERALD

Research School of Earth Sciences, Australian National University, Canberra, ACT 0200, Australia

Abstract—Illite from Muloorina, just south of Lake Eyre in South Australia, is commonly used as a standard ferric iron-bearing illite which has a cation exchange capacity (CEC) of ~22 meq/100 g, too high a value for this clay to conform to the most recent conclusions about illite composition. The objective of the present study was to reassess the Muloorina illite to determine the reason for this high CEC value. The composition determined by X-ray fluorescence analysis calculated to a cation charge of +22 is $K_{0.68}(Mg_{0.39}Al_{1.02}Fe^{3+}_{0.54}Fe^{2+}_{0.04})[Si_{3.59}Al_{0.38}Fe^{3+}_{0.03}]O_{10}(OH)_2$. X-ray diffraction of glycolated and heated K-saturated Muloorina illite revealed no evidence of expandable layers. The cell dimensions are a = 5.314(1) Å, b = 9.040(1) Å, c = 10.135(3) Å, and β = 100.97(3)º (3σ in parentheses). Transmission electron microscopy revealed that Muloorina illite has a remarkably fine and uniform particle size in the form of irregularly stepped hexagonal crystals, averaging 60 nm in diameter at their widest, and 35 nm thick, each step being ~7 nm high. At most steps and between many steps defects occur where a 2:1 layer terminates, with a wide interlayer spacing beyond, commonly reaching to the crystal edge. Even though uninterrupted stacking of >10 or so 2:1 layers across one crystal is uncommon, the irregular distribution of the dislocations leaves appreciable structural continuity so that the mean diffracting thickness is of the order of 16 nm. Muloorina illite is not an interstratified illite-smectite, but a mica mineral with low-charge regions associated with terminating 2:1 layer defects. Such regions are wedge shaped at the nm scale and stabilized by the bonding of the illitic remainder of that interlayer. Approximately 17% of the total volume of each Muloorina illite crystallite is occupied by such low-charge 2:1 layers.

Key Words—Australia, CEC, Defect, Illite, Muloorina.

INTRODUCTION

Illite from Muloorina in central South Australia was first described by Norrish and Pickering (1983) who showed it to be an authigenic, lacustrine, ferric illite, with almost 13 wt.% $FeO+Fe_2O_3$. Since then it has been used in a variety of studies as a type material, and has been found to have a mean particle size of 70 nm, a total specific surface area (TSSA) of ~120 m^2/g, and a cation exchange capacity (CEC) of ~20 meq/100 g (Table 1). Norrish and Pickering (1983) reported the composition of Muloorina illite determined by X-ray fluorescence (XRF) analysis, and their data are included in Table 2.

Few ostensibly similar illites have been described. Keller (1958) described as glauconite a mica having almost exactly the same composition as Muloorina illite from an altered terrestrial volcanic sediment in Montrose County, Colorado, USA. Greenish-gray illite from lacustrine to brackish sediments in the French-Swiss Jura had similar K_2O contents as Muloorina illite but about half as much Fe_2O_3 (Deconinck *et al*., 1988). A ferric illite from non-marine sandstones in Queensland, Australia, was reported by Baker (1997), again with the same composition as Muloorina illite, but the description lacked X-ray diffraction (XRD) data. Authigenic Fe illite-smectites from the Isle of Wight, UK, were described by Huggett *et al*. (2001); the sample from 44 m is essentially smectite-free and has a composition similar to that of Muloorina illite and a particle size ranging down to <100 nm. A ferric illite with similar composition to Muloorina illite was reported by Guimaraes *et al*. (2000), and Longuépée and Cousineau (2006) described as glauconite a clay of almost the same composition. The compositions of most of these ferric illites or glauconites (Table 2) fall in the 'no man's land' between illite and glauconite as defined by the IMA (Rieder *et al*., 1998). Muloorina illite lies at the extreme edge of the illite field ($^{VI}Al/(^{VI}Al+^{VI}Fe^{3+})$ = 0.6.

Muloorina illite appears to be unique in occurring in relative abundance in a monomineralic clay deposit, making the determination of its CEC possible, a measurement lacking in the descriptions of all other ferric illites. By recent definitions of illite, such as that of Meunier and Velde (2004) or Środoń *et al.* (2009), the CEC of Muloorina material is too high, and the K-content too low for it to be end-member illite. These properties raise the possibility that it could be an interstratified illite-smectite, yet none of the previous research detected smectite. The present study was initiated to reassess Muloorina illite.

MATERIALS AND METHODS

All the research reported in the literature involving Muloorina illite used material (collected by John

* E-mail address of corresponding author:
Tony.Eggleton@anu.edu.au
DOI: 10.1346/CCMN.2011.0590606

Table 1. Properties of Muloorina illite, other than composition, from the literature.

CEC (meq/100 g)	Mean particle diameter (nm)	TSSA (m^2/g)	^{IV}Fe	Fe^{2+} (%)	Author
23.7	60	128			Chi *et al.* (1977)
17		137			Greene *et al.* (1978)
			2% of 0.63 Fe p.f.u.	3% of 0.63 Fe p.f.u.	Johnston and Cardile (1987)
		144			Murray and Quirk (1990)
	70			7% of 12.75 wt.% Fe_2O_3	Norrish and Pickering (1993)
		148			Tiller and Smith (1990)
			5% of 0.63 Fe p.f.u.	3.5% of 0.63 Fe p.f.u.	Murad and Wagner (1994)
20.8	68				Barzegar *et al.* (1995)
	64–85				Beckett *et al.* (1997)
	70–90 nm				Noack *et al.* (2000)
	95	123			Lackovic *et al.* (2003)
		107		7% of 0.61 Fe p.f.u.	Seabaugh *et al.* (2006)

CEC: cation exchange capacity; TSSA: total specific surface area; p.f.u.: per formula unit based on $O_{10}(OH)_2$.

Table 2. Chemical analyses of Fe illites.

	Ba-saturated <1 μm XRF	Ba-saturated <<1 μm XRF	Norrish and Pickering (1983)	Ba-saturated <1 μm ATEM*	Keller (1958) Glauconitic mica	Deconinck *et al.* (1988) Bo28	Huggett *et al* (2001) 44 m, <2 μm	Baker (1997) Mean of Group 1 clays	Longuépée and Cousineau (2006) AM-04A (column 2)	Guimaraes *et al.* (2000) Glauconite GRS (column1)
SiO_2	52.3	52.86	52.99	56.1	49.03	56.6	57.19	50.55	54.07	53.6
TiO_2	0.51	0.24	0.31	0.2	1.06	0.58	0.72	N.R.	0.07	0.1
Al_2O_3	17.46	17.41	17.18	16.6	17.93	23.02	16.11	18.17	19.59	12.5
Fe_2O_3	12.46	12.55	11.9	11.9	13.11	7.84	10.41	10.26	11.82	12.8
FeO	N.R.	N.R.	0.94	N.R.	1.31	N.R.	N.R.	1.51	2.36	N.R.
MgO	3.85	3.89	4.16	3.7	2.79	3.73	2.14	2.51	2.39	5.4
CaO	0.13	0.16	0.81	0.1	0.39	0.95	0.07	0.14	0.28	0.1
Na_2O	0.08	0.08		0.1	0.10	0.19	0.16	0.14	0.08	0.1
K_2O	7.72	7.72	7.56	7.4	7.84	7.03	5.03	8.12	7.22	9.4
P_2O_5	0	0	N.R.	N.R.	0.37	N.R.	N.R.	N.R.	N.R.	N.R.
BaO	0.90	0.82	N.R.	N.R.	N.R.	0	0	N.R.	N.R.	N.R.
Rb_2O	0.03	0.03	N.R.	N.R.	N.R.	0	0	N.R.	N.R.	N.R.
H_2O^+	4.19	3.83	4.00*	4.0*	6.00	N.R.	N.R.	N.R.	N.R.	N.R.
Total	99.64	99.61	99.32	100	99.93	99.94	91.83	91.4	98.09	93.9
H_2O^-	4.15	4.29			N.R.	N.R.		N.R.	MNR	N.R.

* 4.00 wt.% H_2O^+ assumed.
N.R.: not reported

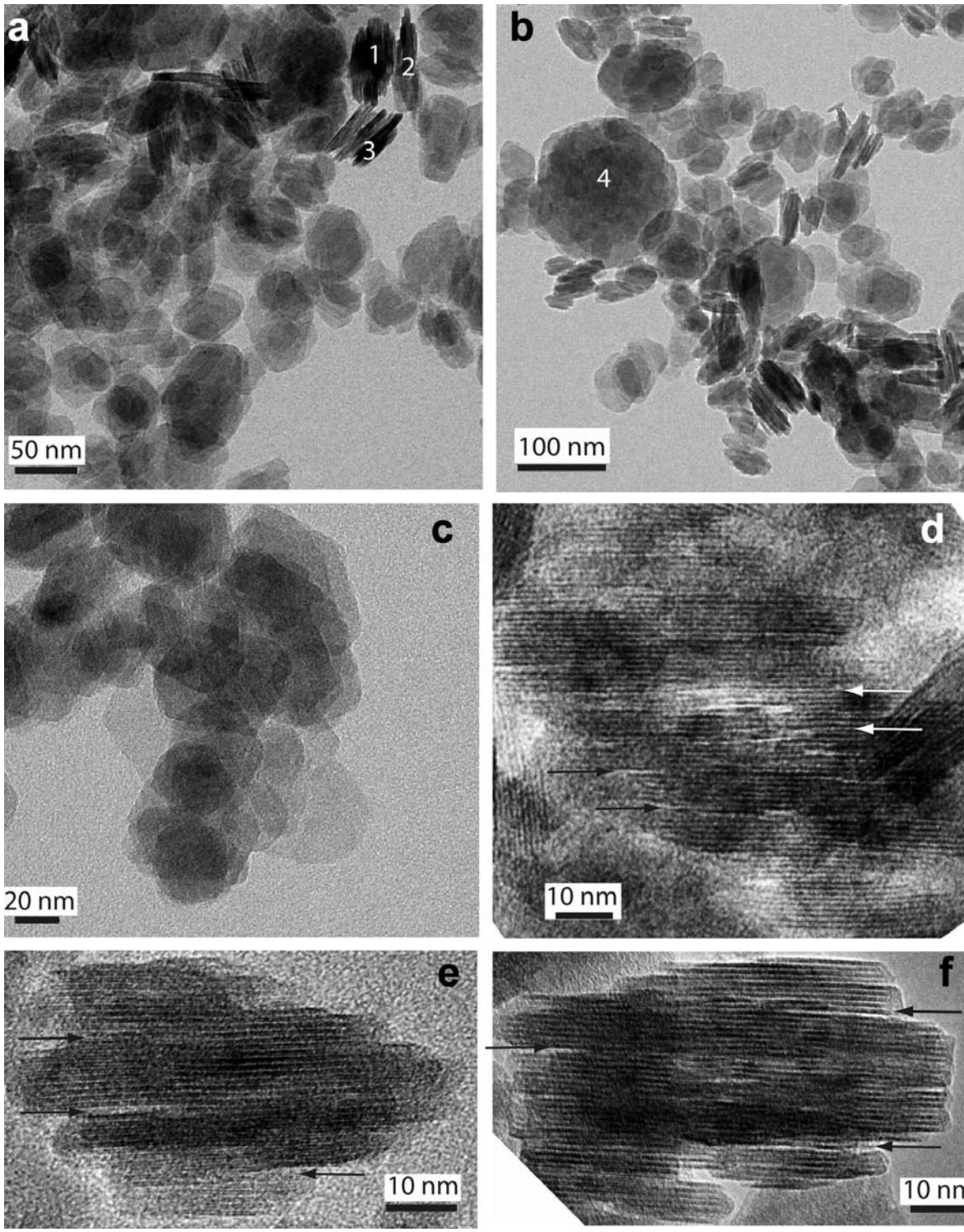

Figure 1. (a–c) Low-magnification TEM images of illite grains dispersed on holey-carbon grids. Note the hexagonal shape of most grains, particularly in part c, and the complex stacking of domains visible in views perpendicular to *z*, *e.g.* those numbered 1, 2 and 3 in part a. Grain 4 in part b, viewed parallel to *z*, shows variable electron absorption attributed to variable thickness. Parts d, e, and f show 1 nm lattice fringes in grains viewed perpendicular to *z*. Part d is an ion-beam thinned sample; parts e and f are grain mounts. Some terminating illite layers are indicated by arrows.

https://doi.org/10.1346/CCMN.2011.0590606 Published online by Cambridge University Press

Pickering and Malcolm Wright) stored at the CSIRO Division of Land and Water, Glen Osmond, South Australia. The illite occurs in the 6 m thick Billa Kalina Clay Member beneath the Millers Creek Dolomite Member of the Etadunna Formation, an Oligocene lacustrine deposit disconformably overlying the glauconitic Cretaceous Bulldog Shale (Jessup and Norris, 1971; Ambrose and Flint, 1981). The illite was collected at a site ~15 km north of Muloorina Station, at the southern edge of Lake Eyre, South Australia. The present study used material from the same repository.

Four random 50 g subsamples were taken from the Muloorina illite, dispersed ultrasonically in distilled water, and the >10 μm fraction extracted by repeated settling for 20 min and removal of the upper 10 cm of suspension. The <10 μm fractions were washed by centrifugation until the clay remained in suspension. From these suspensions the >2 μm fraction was removed by repeated settling. The <2 μm fractions were then K-, Na-, Mg-, or Ba-saturated with 0.1 M chloride solutions, dialyzed with distilled water until the electrical conductivity of the samples was low (<10 μS/m); and, in the case of the Ba-saturated sample, until the Ba content of the dialysis water was <1 ppm. For the Ba-saturated sample, two extracts were obtained by settling, one of <1 μm, the other consisting of clay that had not settled after some days and is referred to hereafter as <<1 μm. Extracts from each sample were deposited on glass slides for XRD analysis, and the Ba-saturated subsample centrifuged and the clay freeze dried. Chemical analysis of the Ba clay was carried out by XRF for major elements and Ba and also by inductively couple plasma-mass spectrometry for Ba, at 'Geoscience Australia' (Canberra). Mass loss on ignition (MLOI) included both adsorbed (H_2O^-) and structural (H_2O^+) water. Both Ba-saturated samples were oven heated at 110ºC to determine the adsorbed water. The CEC was determined by ammonium displacement at the CSIRO Land and Water Laboratories, Glen Osmond, South Australia. The XRD analyses of the original sample and of the Ba-, Mg-, and Na-ion-exchanged clays were carried out using a Siemens D5001 diffractometer with CoKα radiation. Following the approach of Środoń *et al*. (2009), the K-exchanged sample was analyzed on a Siemens D501 diffractometer using CuKα radiation on an oriented aggregate after 24 h of exposure to ethylene glycol vapor at ~60ºC, and again after heating at 250ºC for 24 h. Peak positions for a random mount of the K-saturated illite were determined using *EVA* software (Bruker AXS Gmbh, Germany) after smoothing and cell parameters from this scan computed by least squares (Holland and Redfern, 1997).

For transmission electron microscopy (TEM), a subsample of the Ba-saturated clay powder was set in a block of L R White's resin (Kim *et al.*, 1995) and thin sections microtomed. Grain mounts of Ba- and K-saturated illite were prepared on holey-carbon grids and analyzed by ATEM using a Philips CM300T instrument operating at 300 kV.

RESULTS

Chemistry

The chemical compositions, established by XRF, of the two fractions of Ba-Muloorina illite were very similar to those measured by Norrish and Pickering (1983) (Table 2). The TEM grain-mount images and ATEM revealed the presence of anatase. Prolonged exposure to a focused electron beam showed clearly beam damage and loss of K. The average of two analyses using a broad beam covering many illite crystals, but with no anatase evident, provided an upper limit on the Ti content of the clay (Table 2).

The CEC values for the <1 μm and <<1 μm fractions, established by means of NH_4^+ displacement, were 18.8 and 19.5 meq/100 g, respectively, and by means of XRF analysis of Ba-saturated illite, were 19.9 and 20.1 meq/100 g, respectively.

Transmission electron microscopy

The TEM images of Muloorina illite were used to characterize the morphology and observe details of the lattice (Figure 1a–f). Most of the crystals sedimented onto holey-carbon grids show a roughly hexagonal outline at lower magnification (Figure 1a–c) and hexagonal 0.45 nm lattice fringes at higher magnification (not shown), indicating that they are views down the *z* axis. Other crystals showing 1 nm lattice fringes are views perpendicular to *z* (Figure 1d–f). Crystal thicknesses were measured from such images. Views perpendicular to *z* show most crystals consist of stacks of sub-parallel domains, each domain commonly of different diameter from its neighbor. As reported by others (Table 1), the crystals average 60 nm in diameter (Figure 2a), too small to allow selected area electron diffraction of individuals. The crystals range in thickness from 7 to 100 nm with an average of 35 nm (Figure 2b), and the domains within the crystals are of the order of 6–7 layers thick (Figure 2c). The domains are partly separated by an opening at a defect where a 1 nm 2:1 layer terminates (indicated by arrows in Figure 1d–f and shown diagrammatically and enlarged in Figure 3).

X-ray diffraction

The XRD scan for K-saturated, air-dried Muloorina illite (Figure 4a) matches closely 1*Md* illite (*e.g.* compare with the Silver Hill illite of Drits *et al*., 2010). From the atomic coordinates for Silver Hill illite (Drits *et al*. 2010), modified by the inclusion of Fe in the octahedral sheet, calculated intensities using *CrystalMaker*® (CrystalMaker Software Ltd, Oxford, UK) allowed indices to be assigned to most of the peaks in the Muloorina pattern (Figure 4a), from which unit-cell dimensions were calculated by least-squares means

https://doi.org/10.1346/CCMN.2011.0590606 Published online by Cambridge University Press

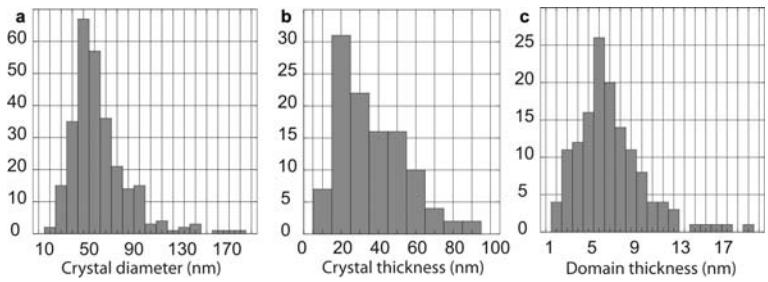

Figure 2. Histograms of Muloorina illite particle sizes measured from TEM images. (a) diameter (nm) (N = 278); (b) thickness (nm) (N = 110); (c) domain thickness (nm) (N = 138).

(Holland and Redfern 1997) using reflections above 20º2θ (Table 3a). The poor resolution of the few indexed *hkl* reflections leaves both the indexing and cell dimensions somewhat uncertain. The scans of glycolated and heated K-saturated illite (Figure 4b, Table 3b), of air-dried and glycolated Mg-saturated illite (Figure 4c), and of air-dried Ca- and Ba-saturated illite (not shown) show no significant differences in terms of 001 peak positions, intensity, or half width.

DISCUSSION

Both Środoń *et al*. (2009) and Meunier and Velde (2004) defined end-member illite in such a way as to preclude the Muloorina material from being end-member illite. The Muloorina illite has insufficient K (0.68 atoms per formula unit (a.p.f.u.) compared with 0.88 a.p.f.u. (Meunier and Velde, 2004) and 0.95 a.p.f.u. (Środoń *et al.*, 2009)). The CEC value for the Muloorina illite is too high (20 meq/100 g, compared to an upper limit of 5 meq/100 g given by both the preceding authors) and makes it a 1*Md* mica, contrary to the Meunier and Velde (2004) definition which requires that illite be 1*M* or $2M_1$. Only in terms of composition does the Muloorina illite conform to the IMA definition of illite (Rieder *et al*., 1998).

Combining these views and definitions suggests that Muloorina illite is an Fe-bearing interstratified illite-smectite. Several tests have failed to support this hypothesis.

Firstly, XRD of the clay deposited from water shows none of the characteristics of interstratified illite/smectite. The basal spacing remains at 10 Å under all treatments and the *00*l XRD peak positions conform within experimental error to those indicated by Środoń *et al*. (2009) for end-member illite. The absence of any significant peak shifts between glycolated and heated Muloorina illite appears to confirm the absence of expandable layers.

Secondly, the particle size of Muloorina illite, as seen in TEM, is unaffected by treatment. Wider particles (*xy* direction) are generally thicker (*z* direction), indicating that the particles do not separate along smectitic interlayers in water suspension.

Thirdly, the TEM images themselves confirm that the particles are connected continuously by K interlayers, albeit in a somewhat zig-zag fashion, throughout their thickness. The 'fundamental particle' of Muloorina illite is the crystal including defects.

From its K content, an estimate of the proportion of high-charge (K) interlayers (illitic) to low-charge interlayers (non-illitic) can be made by assuming that

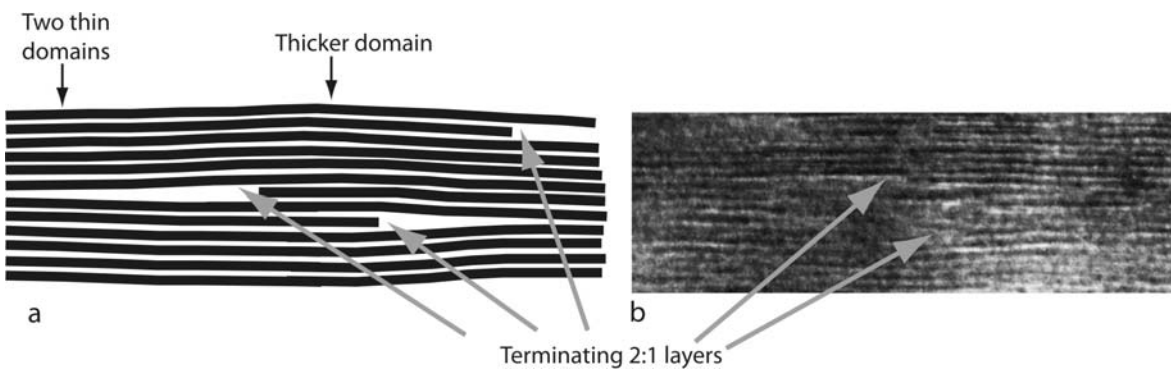

Figure 3. (a) Diagram representing a central thick illite domain separated at a layer-terminating defect into narrower domains left and right with a wider interlayer gap beyond each dislocation. (b) TEM lattice image of Mullorina illite showing terminating 2:1 layers such as those represented in the diagram.

https://doi.org/10.1346/CCMN.2011.0590606 Published online by Cambridge University Press

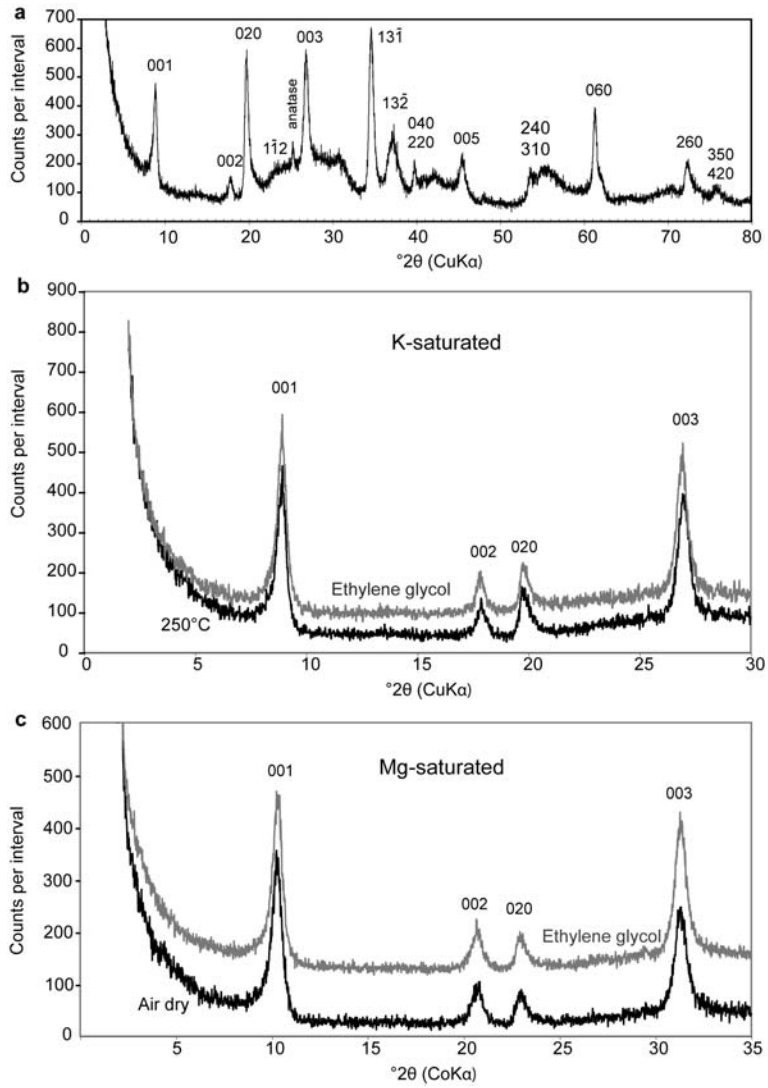

Figure 4. XRD patterns of K-saturated Muloorina illite: (a) random mount, air dried; (b) after glycolation (gray line) and heating to 250ºC (black line); (c) Mg-saturated, air dried (black line), and after glycolation (gray line).

all the K is in mica, the octahedral sheet composition is the same in both components, with the tetrahedral composition (Si, Fe, Al) of the mica component adjusted to yield a charge total of +22. A division of the structural formula into two components on this basis (Table 4) indicates 17% low-charge interlayers. Comparing these end-members to those summarized by Środoń *et al*. (2009), the mica component has appreciably less K than 0.95 a.p.f.u., whereas the low-charge component has exactly the same interlayer charge of 0.41 equivalents p.f.u.

Środoń *et al*. (2009) suggested that the proportion of smectite layers in an illite-smectite can be estimated from the TSSA. Taking the TSSA of a fully hydratable 2:1 layer (such as a smectite layer) as ~750 m^2/g, the TSSA of Muloorina illite of ~130 m^2/g indicates that 17% of its surface is accessible to surface area measurement, *i.e.* 17% of the layers are non-illitic. Środoń *et al*. (2009) also suggested that the fraction of smectite layers = $1/N$, where N is the number of mica layers in the illite fundamental particle. Examination by TEM revealed that Muloorina illite has, on average, one layer defect in every six 2:1 layers, indicating again that 15–20% of the layers have non-illite character.

Beene *et al*. (1991) investigated the electrochemical properties of Muloorina illite and their results indicated that at the pH at which the CEC was measured in this study (8.5), the surface component of the CEC is ~5 meq/100 g. Subtracting that value from the measured CEC of 20 leaves an isomorphous component of 15 meq/100 g, equivalent to 15% non-illitic layers having a CEC of ~100 meq/100 g.

https://doi.org/10.1346/CCMN.2011.0590606 Published online by Cambridge University Press

Table 3a. Diffraction data for K-saturated Muloorina illite.

h	*k*	*l*	d_{obs}	d_{calc}
0	0	1	9.906	9.950
0	0	2	4.957	4.975
0	2	0	4.483	4.520
1	1	$\bar{2}$	3.661	3.658
0	0	3	3.308	3.317
1	3	$\bar{1}$	2.583	2.585
1	3	$\bar{2}$	2.408	2.407
0	4	0	2.259	2.260
2	2	0	2.259	2.259
0	0	5	1.990	1.990
2	4	0	1.705	1.708
3	1	0	1.705	1.708
0	6	0	1.508	1.507
2	6	0	1.303	1.305
3	5	0	1.254	1.253
4	2	0	1.254	1.253

Column d_{calc} computed using a = 5.314(1) Å, b = 9.040(1) Å, c = 10.135(3) Å, β = 100.97(3)º (3σ in parentheses).

Table 3b. 001 peak position and half-width for K-saturated Muloorina illite (CuKα radiation).

	º2θ	Δ2θ
Air dry	8.91	0.47
Glycolated	8.91	0.43
Heated	8.91	0.46

From the XRD results, the thickness of the 00*l* diffracting domains, calculated from the Scherrer equation, is ~16 nm, almost three times the TEM measurement of the illite domain thickness (~6 nm) while being at the low end of the observed crystal thickness (Figure 2b). From the TEM images the Muloorina illite is clearly not entirely separated into 6-layer domains, but occurs as thicker crystals with termination defects visible through the grain spaced on average every six layers. Such terminations have an open region beyond them extending for 10 to 20 nm. Some such openings persist to the crystal edge, others wedge out so that stacking is apparently returned to, or close to, 10 Å layers. One implication from this is that in water these grains do not separate into individual fundamental particles, but always retain their aspect ratio of ~0.4.

The specific surface area of Muloorina illite has been measured by several workers (Table 1). Murray and Quirk (1990), using N_2 adsorption and desorption, obtained values of 144 and 145 m^2/g, respectively, for the total surface area and Chi *et al*. (1977) used both N_2 and H_2O adsorption to arrive at figures for the total surface area of 128 and 125 m^2/g, respectively. The N_2 adsorption method is carried out on dry material in which any expandable (smectitic) layers are collapsed to 10 Å. Therefore, only grain surface area and that of accessible micropores within grains is measured. H_2O, by contrast, enters and expands the interlayer space of expanding clays and so measures both the grain surface area and the expandable interlayer area. The results of Chi *et al*. (1977) suggested that Muloorina illite has no

Table 4. Structural formulae to a cation charge of +22 for Ba-saturated Muloorina illite averaged over the <1 μm and <<1 μm samples of Table 1 and the calculated end-member high-charge (K) and low-charge components of Muloorina clay, assuming that all K is in the high-charge component. Fe species are divided according to the analyses of Norrish and Pickering (1983) and the Mössbauer results of Murad and Wagner (1994).

	Muloorina illite	High-charge (K) component = 83%	Low-charge component = 17%
Si	3.58	3.51	3.91
^{IV}Fe	0.03	0.03	0.03
^{IV}Al	0.39	0.46	0.06
Ti	0.01	0.01	0.01
Al	1.01	1.01	1.01
Fe^{3+}	0.58	0.58	0.58
Fe^{2+}	0.04	0.04	0.04
Mg	0.39	0.39	0.39
Octahedral site occupancy	2.03	2.03	2.03
Octahedral charge	5.67	5.67	5.67
K	0.67	0.81	0.00
Na	0.01	0.01	0.01
Ca	0.01	0.00	0.06
Ba	0.02	0.00	0.13
Rb	0.00	0.00	0.01

https://doi.org/10.1346/CCMN.2011.0590606 Published online by Cambridge University Press

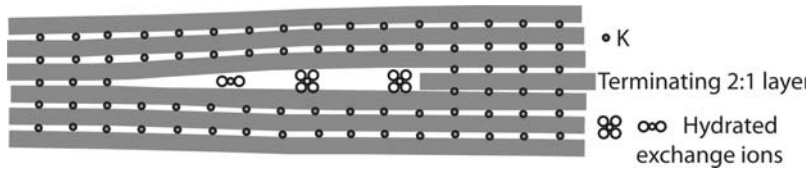

Figure 5. Diagram representing hydrated exchange ions in the gap between 2:1 mica layers where a layer terminates.

expandable layers, because water adsorption found no greater surface area than did N_2 adsorption. The wedge-shaped voids evident in the TEM images provide ample space for the ingress of water without any associated expansion of the interlayer region, because they are already up to 1 nm wide (Figure 5).

From the particle-size data for the average diameter and thickness of the crystals, and assuming each crystal has the stepped morphology of those shown in Figure 1d–f, the calculated grain surface area is ~80 m^2/g, considerably less than the N_2-measured total surface area (average 131 m^2/g). The wider interlayer space at a termination defect would be accessible to N_2 and water if it extended to the grain edge, and allowance for such defects would increase the calculated surface area.

A defect with its edge normal to the beam direction, such as the lower terminating plane in the diagram of Figure 6, would be difficult to detect, though its

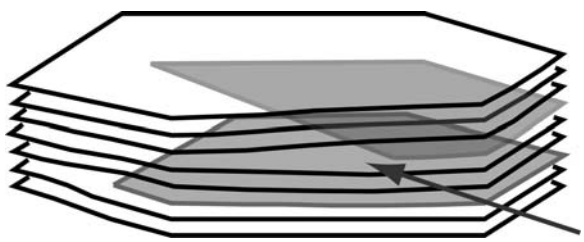

Figure 6. Diagram representing two terminating 2:1 layers with their edges in different orientations. A view in the direction of the arrow would see only the upper terminating layer.

presence might be suggested in high-resolution images by blurring of the 10 Å fringes. Such loss of clarity is abundant in the images and in many cases interfered with attempts to count sequences of uninterrupted layers. In order not to bias the count, such areas were treated as continuous and the count made elsewhere on the crystal where no loss of clarity occurred. This will have led to underestimation of the number of defects, but because any view parallel to 001 reveals the same frequency of terminations, the total surface area within the crystals open to N_2 or H_2O is much the same as would be the case for isolated 6- to 7-layer crystals. The calculated surface area of such a configuration is 140 m^2/g, in good agreement with the measured value.

CONCLUSIONS

The combined evidence suggests that ~17% of the interlayer region of Muloorina illite is not occupied by K but holds exchange ions and adsorbed water. The lack of continuity of these interlayers and the rigidity of the adjacent illite component prevents expansion of these regions in the normal manner of a smectite. This in turn suggests that Muloorina illite is not an interstratified illite-smectite as such materials are normally considered to be, but is an illite with a large percentage of 001 layer-termination defects, such that ~17% of its interlayer region contains exchangeable cations, with a resulting reduction in K content. Figures 5 and 6 represent this structure in diagrammatic form.

ACKNOWLEDGMENTS

The authors thank the staff at CSIRO Land and Water, Adelaide, for access to the Muloorina Illite repository, and Richard Greene for helpful discussions about particle-size analysis. F. Nieto and an anonymous reviewer are thanked for helping to improve the manuscript. The authors are grateful for access to TEM equipment at the Centre for Advanced Microscopy in the Australian National University, a node of the Australian Microscopy and Microanalysis Research Facility.

REFERENCES

Ambrose, J.G. and Flint, R.B. (1981) A regressive Miocene lake system and silicified strandlines in northern South Australia: implications for regional stratigraphy and silcrete genesis. *Journal of the Geological Society of Australia*, **28**, 81–94.

Baker, J.C. (1997) Green ferric clay in non-marine sandstones of the Rewan Group, southern Bowen Basin, eastern Australia. *Clay Miner*als **32**, 499–506.

Barzegar, A.R., Oades, J.M., Rengasamy, P., and Murray, R.S. (1995) Tensile strength of dry, remoulded clays as affected by properties of the clay fraction. *Geoderma*, **65**, 93–108.

Beckett, R., Murphy, D., Tadjiki, S., Chittleborough, D.J., and Giddings, J.C. (1997) Determination of thickness, aspect ratio and size distributions for platey particles using sedimentation field-flow fractionation and electron microscopy. *Colloids and Surfaces A*, **120**, 17–26.

Beene, G.M., Bryant, R., and Williams, D.J.A. (1991) Electrochemical properties of illite. *Journal of Colloid and Interface Science*, **147** 358–369.

Chi, C.L., Emerson, W.W., and Lewis, D.G. (1977) Exchangeable calcium, magnesium and sodium and the dispersion of illites in water. I. Characterization of illites and exchange reactions. *Australian Journal of Soil Research* **28**, 243–253.

Deconinck, J.F., Strasser, A., and Debrabant, P. (1988)

Formation of illitic minerals at surface temperatures in Purbeckian sediments (Lower Berriasian, Swiss and French Jura). *Clay Minerals*, **23**, 91–103.

Drits, V.A., Zviagina, B.B., McCarty, D.K., and Salyn, A.L. (2010) Factors responsible for crystal-chemical variations in the solid solutions from illite to aluminoceladonite and from glauconite to celadonite. *American Mineralogist*, **95**, 348–361.

Greene, R.S.B., Posner, A.M., and Quirk, J.P. (1978) A study of the coagulation of montmorillonite and illite suspensions by calcium chloride using the electron microscope. Pp. 35–40 in: *Modification of Soil Structure* (W.W. Emerson, R.D. Bond, and A.R. Dexter, editors). John Wiley, New York.

Guimaraes E., Velde, B., Hillier, S., and Nicot, E. (2000) Diagenetic/anchimetamorphic changes in the Proterozoic glauconite and glaucony from the Paranoa Grour mid-western Brazil. *Revista Brasileira de Geosciências*, **30**, 363–366.

Holland, T.J.B. and Redfern, S.A.T. (1997) *UNITCELL*: a nonlinear least-squares program for cell-parameter refinement and implementing regression and deletion diagnostics. *Journal of Applied Crystallography*, **30**, 84.

Huggett, J.M., Gale, A.S., and Clauer, N. (2001) The nature and origin of non-marine 10 Å clay from the Late Eocene and Early Oligocene of the Isle of Wight (Hampshire Basin), UK. *Clay Minerals*, **36**, 447–364.

Jessup, R.W. and Norris, R.M. (1971) Cainozoic stratigraphy of the Lake Eyre Basin and part of the arid region lying to the south. *Journal of the Geological Society of Australia*, **18**, 303–331.

Johnston, J.H. and Cardile, C.M. (1987) Iron substitution in montmorillonite, illite, and glauconite by ^{57}Fe Mössbauer spectroscopy. *Clays and Clay Minerals*, **35**, 170–176.

Keller, W.D. (1958) Glauconitic mica in the Morrison Formation in Colorado. *Clays and Clay Minerals*, **5**, 120–128.

Kim, J.W., Peacor, D.R., Tessier, D., and Elsass, F. (1995) A technique for maintaining texture and permanent expansion of smectite interlayers for TEM observations. *Clays and Clay Minerals*, **43**, 51–57.

Lackovic, K., Angove, M.J., Wells, J.D., and Johnson, B.B. (2003) Modeling the adsorption of Cd(II) onto Muloorina illite and related clay minerals. *Journal of Colloid and Interface Science*, **257**, 31–40.

Longuépée, H. and Cousineau, P.A. (2006) Constraints on the genesis of ferrian illite and aluminium-rich glauconite: Potential impact on sedimentology and isotope studies. *The Canadian Mineralogist*, **44**, 967–980.

Meunier, A. and Velde, B. (2004) *Illite: Origins, Evolution and Metamorphism*. Springer-Verlag, Berlin, 286 pp.

Murad, E. and Wagner, U. (1994) The Mössbauer spectrum of illite. *Clay Minerals*, **29**, 1–10.

Murray, R.S. and Quirk, J.P. (1990) Surface area of clays. *Langmuir*, **6**, 122–124.

Noack, A.G., Grant, C.D., and Chittleborough, D.J. (2000) Colloid movement through stable soils of low exchange capacity. *Environmental Science & Technology*, **34**, 2490–2497.

Norrish, K. and Pickering, J.G. (1983) Clay minerals. Pp. 281–308 in: *Soils: an Australian Viewpoint.* Division of Soils CSIRO, Melbourne and Academic Press, London.

Rieder, M., Cavazzini, G., D'Yakanov, Y.S., Frank-Kamentskii, V.A., Gottardi, G., Guggenheim, S., Koval, P.V., Müller, G., Neiva, A.M.R., Radoslovich, E.R., Robert, J.-L., Sassi, F.P., Takeda, H., Weiss, Z., and Wones, D.R. (1998) Nomenclature of the micas. *The Canadian Mineralogist*, **36**, 905–912.

Seabaugh, J.L., Dong, H., Kukkadapu, R.K., Eberl, D., Morton, J.P., and Kim, J.W. (2006) Microbial reduction of Fe(III) in the Fithian and Muloorina illites: contrasting extents and rates of bioreduction. *Clays and Clay Minerals*, **54**, 67–79.

Środoń, J., Zeelmaekers, E., and Derkowski, A. (2009) The charge component of layers of illite-smectite in bentonites and the nature of end-member illite. *Clays and Clay Minerals*, **57**, 649–671.

Tiller, K.G. and Smith, L.H. (1990) Limitations of EGME retention to estimate the surface area of soils. *Australian Journal of Soil Research*, **28**, 1–26.

(*Received 28 February 2011; revised 12 October 2011; Ms. 550; A.E. S. Petit*)